Table 1 Thick cylinder subjected to unit internal pressure—displacements and stresses[a]

Radius,	Displacement, $u \times 10^{-7}$ in.		Stresses, lb/in.^{2}							
			σ_x			σ_θ			σ_y	
in.	Present element[b]	Exact[7]	Present element	Exact	Ref. (8)[c]	Present element	Exact	Ref. (7)	Present element	Exact
1.0	1.9066	1.9066	−0.9797	−1.0	−0.840	1.6755	1.6667	1.734	0.2087	0.2000
1.5	1.4157	1.4156	−0.2582	−0.2593	−0.262	0.9264	0.9259	0.925	0.2004	0.2000
2.0	1.2133	1.2133	−0.0027	0.0000	−0.028	0.6654	0.6667	0.657	0.1988	0.2000

[a] Geometry: external radius/internal radius = 2.0; $E = 10^7$ lb/in.^{2}; $\nu = 0.3$; internal pressure = 1 lb/in.^{2}; u = radial displacement; σ_x = radial stress; σ_y = axial stress; and σ_θ = tangential stress. [b] Matrix order 12. [c] Matrix order 63 (using the six-degree-of-freedom finite element of Ref. 3).

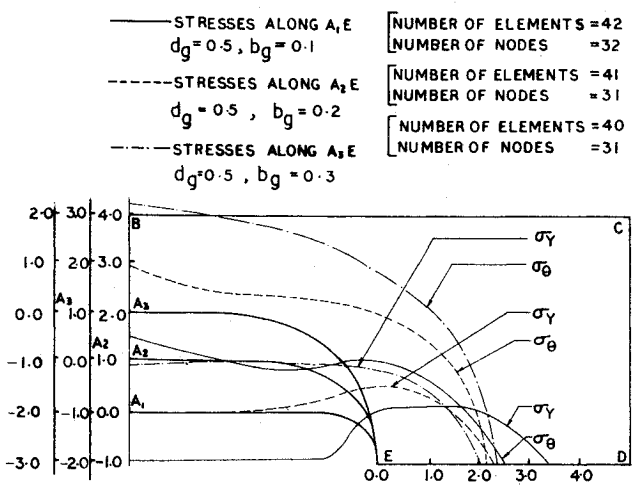

Fig. 4 Stress distribution along A_1E, A_2E and A_3E.

respectively. The theoretical value of Neuber[6] for an infinite shaft is 2.175. The agreement between these solutions is satisfactory.

Thick Cylinders with Internal Semicircular Grooves

Figure 2 shows a long thick cylinder with equally spaced semi-circular grooves, subjected to internal pressure of unity. The ratio of the external radius to the internal radius (r_o/r_i) of the cylinder is taken as two. The spacing between the center lines of the grooves $2b$ is taken as 1. $2b_g$ is the depth of the groove and d_g is the length of the groove in the radial direction. Since the cylinder is assumed long with equally spaced grooves, only the portion ABCDE is considered for the analysis applying proper boundary conditions on the edges BC and DE as shown in Fig. 2.

Two parametric studies are made in this Note: 1) keeping b_g to be 0.25, d_g is varied from 0.25, 0.5 to 0.75; and 2) keeping d_g to be 0.5, b_g is varied from 0.1, 0.2 to 0.3. The stresses σ_y and σ_θ are obtained along the edge AE for the preceding cases and are presented in Figs. 3 and 4, respectively. To obtain accurate stresses along the edge AE, a fine finite element mesh is taken around the groove. It can be concluded from Fig. 3 that as d_g is increased σ_y and σ_θ increases marginally at the point E where as at the point A there is a significant increase of σ_θ. From Fig. 4, it can be noted that as b_g increases, at point E there is not much appreciable change in the value of σ_θ, but σ_y decreases significantly. σ_y at point A should be -1 because of the applied unit internal pressure and is correctly predicted by the present finite element analysis.

Conclusions

The high-precision axisymmetric solid ring element[4] is used in analyzing the stresses around the internal semi-circular grooves of a typical thick cylinder such as a kick motor of a 4 stage rocket subjected to internal pressure. The application of the present element in Lame's problem shows the extreme accuracy of the finite element used. Even though the analysis presented in this Note is for simple groove geometries, the present finite element can be confidently applied to the analysis of complicated internal grooves, which are actually encountered in the design of rocket motor grains.

References

[1] Glick, R. L. and Thurman, J. L., "An Analysis of the Circumferential Slot Effects on the Internal Ballistics of the TX 354 Motor," Special Rept. U-65-11A, Feb. 1965, Thiokol Chemical Corp., Huntsville, Ala.

[2] Fourney, M. E., "A Pseudo Two-Dimensional Photoelastic Method of Testing Axisymmetric Geometries," *Journal of the Society for Experimental Stress Analysis,* 1971, pp. 19-25.

[3] Zienkiewiez, O.C., *The Finite Element Method in Engineering Science,* McGraw-Hill, London, 1971.

[4] Venkateswara Rao, G. and Prakasa Rao, B., "A High-Precision Triangular Ring Element for the Analysis of Axisymmetric Solids," *Journal of the Aeronautical Society of India,* (to be published).

[5] Raju, I. S. and Murthy, T. V. G. K., "An Algorithm for Integration in Triangular Domains," *Journal of the Aeronautical Society of India,* Vol. 25, 1973, pp. 40-42.

[6] Neuber, H. and Edwards, J. W., *Theory of Notch Stresses,* University of Michigan Press, Ann Arbor, Mich., 1946, p. 84.

[7] Venkataraman, B. and Patel, S. A., *Structural Mechanics with Introduction to Elasticity and Plasticity,* McGraw-Hill, London, 1970.

[8] Raju, I.S. and Avasthi, S. C., "Axisymmetric Ring Element of Triangular Cross-section-TRIAX-3 Elements," 1972, Tech. Rept., Structural Engineering Div., Space Science and Technology Centre, Trivandrum, India.

Assessment of Pressure Port Erosion Effects

J.M. Cassanto*
General Electric Company, Philadelphia, Pa.

I. Introduction

EROSION around forebody pressure port holes on R/V's employing ablative heat shields can cause erroneous flight test pressure to be recorded in turbulent flow. The erroneous pressures can be misinterpreted during the post flight analysis causing invalid conclusions to be drawn regarding the R/V performance.

Forebody pressure data are required to meet the mission objectives/goals of most R&D R/V flight test programs by determining the inflight forebody drag component of total drag. Accordingly, it is important to assess the effects of

Presented as Paper 75-150 at the AIAA 13th Aerospace Sciences Meeting, Pasadena, California, January 20-22, 1975; submitted February 20, 1975; revision received June 23, 1975. The author would like to gratefully acknowledge the assistance of the following persons who contributed to the various test programs utilized in this paper: F.C. George; S. Stadelmeier; D.R. Stewart; A. Saydah; C. Fehl; J. Botje; N. Satin; R. Neff; T. Hoyt; and P. Browne.

Index categories: Entry Vehicles and Landers; LV/M Flight Testing; Supersonic and Hypersonic Flow.

*Project Engineer, Re-Entry and Environmental Systems Division. Member AIAA.

pressure port erosion on the measured flight test pressure data, and/or to minimize erosion effects.

The purpose of this Note is twofold: First, to present the results of an experimental program employing both ground and flight test data to evaluate pressure port erosion effects; second, to propose two potential solutions/fixes to the erosion problem.

II. Ground Test Results

Pressure data on ablating heat shields were obtained from the Malta rocket exhaust facility. The tests were conducted on virgin full scale carbon phenolic (CP) heat shields at angle of attack. The rocket was fired in an open test stand (at ambient pressure) and had an exhaust Mach number of $M_\infty \approx 2.5$. Pressure ports consisted of simple 0.060 in. diam holes drilled through the heat shield for two types of CP heat shield fabrication modes. The test duration was ~20 sec, and pressure ports were located on the windward meridian. The pressure ports were examined and photographed after the tests to determine if the ports eroded. The boundary layer was turbulent for all tests based on calorimeter data.

Data for a typical test are presented in Fig. 1 and clearly show that the port that eroded produced a decaying pressure time history while the port that did not erode produced a relatively constant pressure time history. The eroded port indicated ~25% lower pressure than the "clean" port at the end of the run. Port erosion for the low helix angle CP heat shield appeared to be a random nonrepeatable process during the test series. Two ports out of nine showed severe erosion (gouging) on the downstream lip aft of the port. One port showed minor erosion.

Several important additional trends/observations were noted from the Malta and other arc results test series. First, erosion appears to be a function of heat shield fabrication mode. This is verified by tests conducted on high helix angle CP heat shields which showed no erosion for the test series which consisted of four pressure ports. Second, erosion appears to be a function of pressure port diameter: large port diameters ($d \approx 0.100$ in.) always show erosion/gouging while smaller ports ($d = 0.060$ in.) show erosion only part of the time, and finally it is considered that very small ports ($d \approx$ 0.030 in.) would not experience erosion. Third, erosion appears to be a function of heat shield material for a given port diameter, e.g., large mass addition rate/ablation materials such as Teflon, epoxy, and phenolic refrasil are prone to pressure port erosion while low mass addition rate materials such as carbon and graphitics are less prone to port erosion effects.

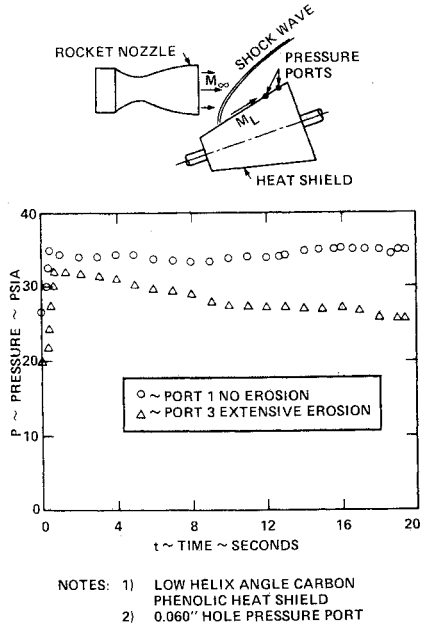

Fig. 1 Pressure time history for ablating heat shield showing pressure port erosion effects.

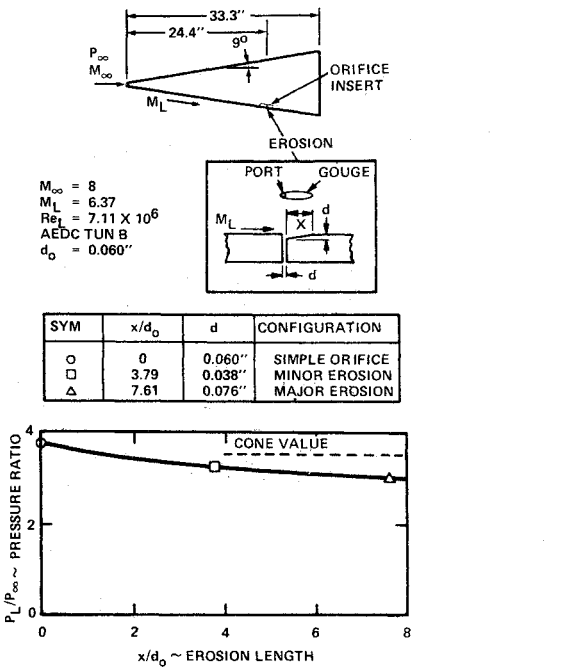

Fig. 2 Wind tunnel data showing the effect of simulated erosion on measured pressure.

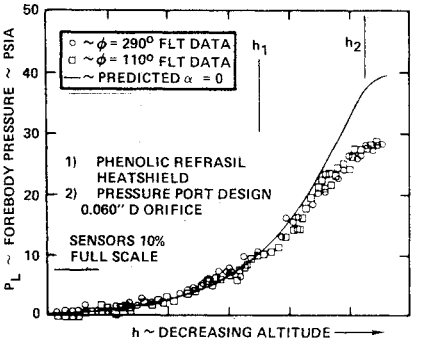

Fig. 3 Forebody flight test pressure data showing significant pressure port erosion effects in turbulent flow (port diam = 0.060 in.)

Wind tunnel pressure tests[1] were also conducted at AEDC tunnel B to evaluate port erosion effects. The model was a slender cone with "quick change" plug orifice inserts to simulate port erosion effects. Test conditions were: $M_\infty = 8$, $\alpha = 0$, $Re_L = 7.1 \times 10^6$, turbulent flow. Figure 2 presents pressure data results for gouges behind a pressure port which simulate erosion of the downstream lip. The data clearly show that the measured pressure decreases as the eroded area increases. The data show that the indicated pressure for the large gouge is ~20% lower than for a simple 0.060 in. diam hole, and is consistent with the Malta test rocket exhaust test data.

III. Flight Test Results

Flight test pressure data have been obtained on a re-entry vehicle with a phenolic refrasil heat shield that was recovered. These data provide the unique opportunity to correlate flight test pressure measurements with heat shield erosion patterns around the pressure ports.

The pressure measurements were obtained with a simple 0.060 in diam hole pressure port. The R/V was a slender cone, which had a low angle of attack (less than 1°) during the data taking period. A typical pressure history for diametrically opposed pressure ports at the aft station of the R/V is presented in Fig. 3. Note that the pressure data from both transducers are in good agreement with the predicted pressure level in laminar flow, altitude h_l. However, for altitudes lower than h_l (turbulent flow), the measured pressure data start to

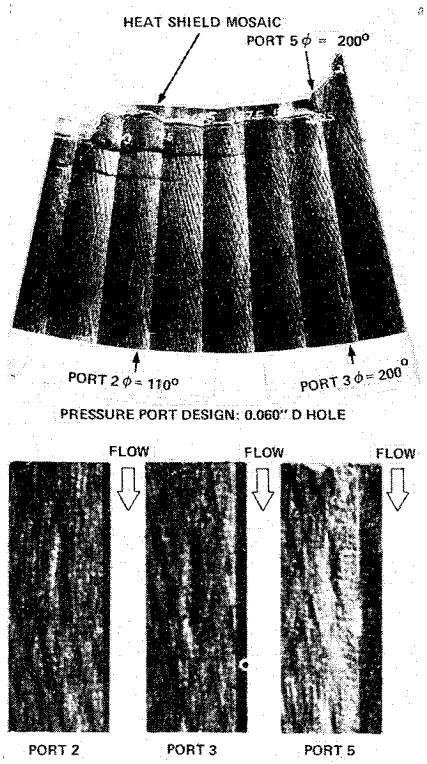

Fig. 4 Recovered heat shield showing eroded pressure ports.

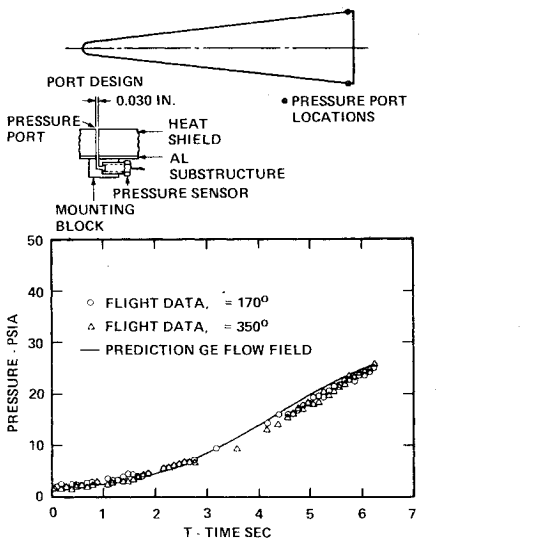

Fig. 5 Pressure sensor/port flight experiment showing negligible erosion effects in laminar and turbulent flow (port diam = 0.030 in.)

diverge, and are ~25-30% lower than predicted.[2] The heat shield contained seven pressure ports, and all showed this same approximate trend. It is concluded that the pressure ports started to erode at altitude h_1 and continued to erode until the end of the flight ($h < h_2$).

This conclusion is verified by typical photographs of the recovered heat shield (Fig. 4) which clearly show erosion effects. Extensive erosion on the downstream lip of the pressure ports is evident by the large "gouges" that occur downstream of each pressure port. The gouge lengths vary from ~12-20 pressure port diameters and gouge depths were ~10-15 mils.

An experiment[3] was conducted to demonstrate the feasibility of a new type of solid state pressure transducer in a flight test application, and to demonstrate that pressure port erosion effects could be minimized with a small diameter port. The flight experiment was conducted on a re-entry vehicle similar to the R/V utilized to obtain the data from Figs. 3 and 4. The R/V configuration, trajectory, and heat shield

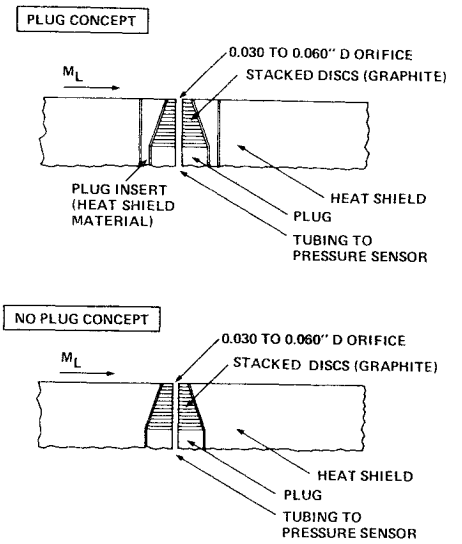

Fig. 6 Stacked disk pressure port design for ablative heat shields.

material were similar. The port diameter, however, was reduced to 0.030 in. diam.

The reduced flight data for diametrically opposed ports are presented in Fig. 5. The data can be seen to be in basic agreement with the GE flowfield solution. For time less than ~3 sec the agreement is excellent. For times between 4 to 6 sec the data are slightly lower than the predicted level. This discrepancy is believed due to slight pressure port erosion effects. It should be noted, however, that the magnitude of the discrepancy (~5%) between measured and predicted flight pressure data is much less than for the discrepancy of data from Fig. 3 (~30% for 0.060 in. diam ports) of this note. Accordingly, it is concluded that pressure port erosion effects can be minimized by utilizing a small pressure port diameter.

IV. Recommended Solution

Two solutions exist to the pressure port erosion problem in turbulent flow. Flight test data have indicated that pressure port erosion can be minimized[4] by reducing the port diameter to ~0.030 in. diam. Pressure port erosion effects, however, can be eliminated by employing the "stacked disk" pressure port concept. The concept consists of stacked disks arranged in a frustum and placed in the heat shield with the smallest disk closest to the outer heat shield surface as shown in Fig. 6. The design works in the following manner: prior to any ablation, the top disk is nearly coincident with the heat shield surface. As the heat shield ablates, the disks "flip" off sequentially keeping pace with the recession rate of the heat shield. This exposes a new surface with a sharp orifice approximately every second thus eliminating erosion effects.

In addition, this pressure port design also tends to eliminate burrs at the pressure port and "clogging" of the port for heat shield materials that tend to melt and run. This design has been flown on several GE-RESD flight vehicles/programs having ablative heat shields and has provided high quality flight data. The decision to implement the "stacked disk" pressure port design represents a tradeoff between cost and data quality that each flight test engineer must evaluate. If ~5 to 10% data is acceptable, the small port diameter (~0.030 in. diam) appears to yield good results (Fig. 5); however, if higher quality flight data are required, the more costly stacked disk design is recommended.

References

[1] Cassanto, J.M., "Effects of Orifice Geometry on Measured Pressures," General Electric Company, Re-Entry and Environmental Systems Products Division, Aerodynamics Laboratory Data Memo, ALDM 68-72, Oct. 1968, General Electric Co., Philadelphia, Pa.

[2]Gravalos, F.G., Edelfelt, I.H., and Emmons, H., "The Supersonic Flow About Blunt Bodies of Revolution for Gases at Chemical Equilibrium," General Electroc Company, Missile and Space Division, TIS R58SD245, June 1959, General Electric Co., Philadelphia, Pa.

[3]Cassanto, J.M., Rogers, D.A., Droms, C.R., and Robison, A.G., "Use of a Miniature Solid State Pressure Transducer for R/V Flight Test Application," *Proceedings of 20th International Instrumentation Symposium*, Albuquerque, N.M., 1974.

[4]Cassanto, J.M., "R/V Flight Test Pressure Instrumentation Techniques," Paper presented at 8th Transducer Workshop, Dayton, Ohio, April 1975.

Effects of Porous Rings on the Aerodynamic Characteristics of a Sphere

George L. Cahen*
Martin Marietta Corporation, Denver Colo.

Nomenclature

A_{ref}	= reference area, $\pi d^2/4$
d	= diameter of sphere
D	= outer diameter of ring
q	= dynamic pressure, $\rho V^2/2$
V	= velocity
C_D	= drag coefficient, drag force / qA_{ref}
C_L	= lift coefficient, lift force / qA_{ref}
C_M	= pitching moment coefficient, pitching moment / $qA_{ref}d$
C_N	= normal force coefficient, normal force / qA_{ref}
α	= angle of attack
σ	= radius of gyration in pitch
$C_{L_\alpha} C_{M_\alpha}, C_{N_\alpha}$	= derivatives with respect to α
$\partial C_M/\partial(\theta d/2V)$ $+\partial C_M/\partial(\dot{\alpha} d/2V)$	= pitch damping coefficient. Overdot implies derivative with respect to time.

Introduction

THE erratic behavior of a sphere in free flight is well known; the fluid mechanical phenomenon—vortex shedding—which is responsible for this behavior is quite well understood. However, to utilize the structural advantage of a sphere for high-pressure planetary entries, it is desirable to improve the stability characteristics and increase its drag coefficient to control the rate of descent. In search of such a solution, Martin Marietta, with NASA's Ames and Langley Research Centers, has tested (both statically and dynamically) a number of concepts. These have included flares, split flares, vented flares, thin rings, both equatorially and post equatorially located, and thick (0.05d), porous rings, equatorially located (originally suggested by NASA Ames Research Center).

The three component static tests measured axial force, normal force and pitching moment in the Martin Marietta, Denver, subsonic wind tunnel. Two types of dynamic tests were conducted. In one the models were mounted on a wire stretched horizontally across the test section of the Army Meteorological Wind Tunnel at Colorado State University so that they were free to pitch through 360°. The other dynamic test was conducted in a vertical wind tunnel (NASA Langley Spin Tunnel) in which the models were free to move in six degrees-of-freedom. Of all configurations tested, the thick porous ring was the most practical. Therefore, this Note will present only the results obtained for that configuration. The effects of ring to sphere diameter ratio, porosity, and center of gravity (c.g.) location on the directional stability and of hole cant angle on the roll rate will be discussed.

Received March 24, 1975; revision received May 27, 1975.
Index categories: Entry Deceleration Systems and Flight Mechanics (e.g., Parachutes); Entry Vehicle Dynamics and Control.

*Senior Group Engineer. Associate Fellow AIAA.

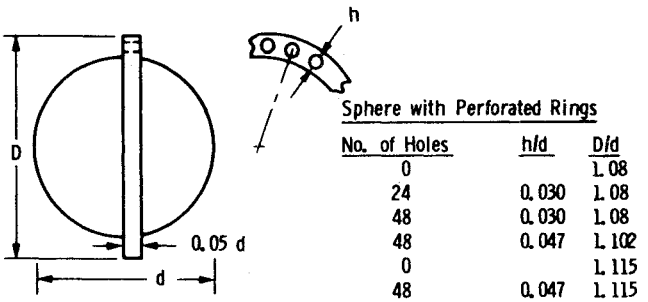

Fig. 1 Configurations tested in the Martin Marietta subsonic wind tunnel.

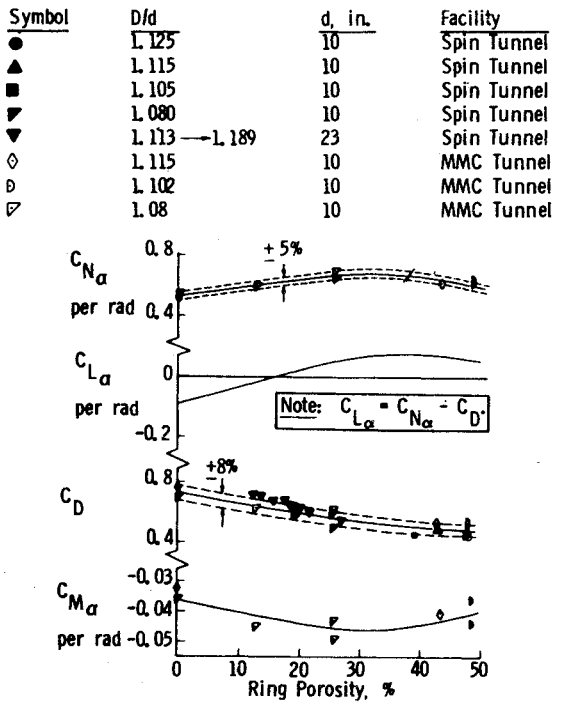

Fig. 2 Summary of aerodynamic derivatives and drag coefficients for zero angle of attack.

Results and Discussion

Static Tests

The configurations for which three component static data were measured are shown in Fig. 1. The sphere model was 10 in. in diameter and constructed of thin (about 1/32 in.) fiberglass reinforced plastic with an aluminum adaptor for sting mounting on a conventional strain gage balance. The porous rings were made of balsa wood. Figure 2 summarized the drag coefficients and the aerodynamic derivatives for $\alpha = 0$ as functions of ring porosity for all configurations tested. Note that, although the data are plotted as functions of porosity, the effects of ring diameter and porosity are both included. For more detailed examination, the pure effect of porosity can be seen for the cases of $D/d = 1.080$ and 1.115. The data show that variations in ring geometry can be used to control the sphere aerodynamic characteristics over a considerable range. The lift curve slope varies with porosity from negative to positive; the drag varies significantly with porosity